HHS Public Access

Author manuscript

Magn Reson Med. Author manuscript; available in PMC 2021 October 01.

Published in final edited form as:

Magn Reson Med. 2021 April ; 85(4): 2174–2187. doi:10.1002/mrm.28561.

Highly accelerated aortic 4D flow MRI using compressed sensing: Performance at different acceleration factors in patients with aortic disease

Ashitha Pathrose[1], **Liliana Ma**[1,2], **Haben Berhane**[3], **Michael B. Scott**[1,2], **Kelvin Chow**[1,4], **Christoph Forman**[5], **Ning Jin**[4], **Ali Serhal**[1], **Ryan Avery**[1], **James Carr**[1,2], **Michael Markl**[1,2]

[1]Department of Radiology, Feinberg School of Medicine, Northwestern University, Chicago, Illinois, USA

[2]Department of Biomedical Engineering, Northwestern University, Evanston, Illinois, USA

[3]Department of Medical Imaging, Ann & Robert H. Lurie Children's Hospital of Chicago, Chicago, Illinois, USA

[4]Cardiovascular MR R&D, Siemens Medical Solutions USA, Inc., Chicago, Illinois, USA

[5]Siemens Healthcare, Erlangen, Germany

Abstract

Purpose: To systematically assess the feasibility and performance of a highly accelerated compressed sensing (CS) 4D flow MRI framework at three different acceleration factors (R) for the quantification of aortic flow dynamics and wall shear stress (WSS) in patients with aortic disease.

Methods: Twenty patients with aortic disease (58 ± 15 y old; 19 M) underwent four 4D flow scans: one conventional (GRAPPA, R = 2) and three CS 4D flows with R = 5.7, 7.7, and 10.2. All scans were acquired with otherwise equivalent imaging parameters on a 1.5T scanner. Peak-systolic velocity (V_{max}), peak flow (Q_{max}), and net flow (Q_{net}) were quantified at the ascending aorta (AAo), arch, and descending aorta (DAo). WSS was calculated at six regions within the AAo and arch.

Results: Mean scan times for the conventional and CS 4D flows with R = 5.7, 7.7, and 10.2 were 9:58 ± 2:58 min, 3:40 ± 1:19 min, 2:50 ± 0:56 min, and 2:05 ± 0:42 min, respectively. V_{max}, Q_{max}, and Q_{net} were significantly underestimated by all CS protocols (underestimation ≤ −7%, −9%, and −10% by CS, R = 5.7, 7.7, and 10.2, respectively). WSS measurements showed the highest underestimation by all CS protocols (underestimation ≤ −9%, −12%, and −14% by CS, R = 5.7, 7.7, and 10.2).

Conclusions: Highly accelerated aortic CS 4D flow at R = 5.7, 7.7, and 10.2 showed moderate agreement with the conventional 4D flow, despite systematically underestimating various

Correspondence: Ashitha Pathrose, Department of Radiology, Northwestern University, 737 N Michigan Ave, Suite 1600, Chicago, IL 60611, USA. ashitha.pathrose@northwestern.edu.

SUPPORTING INFORMATION

Additional Supporting Information may be found online in the Supporting Information section.

hemodynamic parameters. The shortened scan time may enable the clinical translation of CS 4D flow, although potential hemodynamic underestimation should be considered when interpreting the results.

Keywords

aorta; cardiovascular; compressed sensing; 4D flow

1 | INTRODUCTION

Three-dimensional time-resolved cine phase-contrast MRI with three-directional velocity encoding, also known as 4D flow MRI, has evolved rapidly over the past several decades, with its utility as an investigational tool expanding into a wider clinical role in the recent past. When used in cardiovascular imaging, 4D flow MRI helps in the evaluation and characterization of various congenital[1–4] and adult heart diseases,[5–8] particularly several aortic diseases.[9–12] The unique ability of 4D flow MRI to measure advanced metrics such as flow energetics and wall shear stress (WSS) has given newer insights into disease pathophysiology that could not be obtained through other existing imaging modalities.[13–17] However, these benefits come at the expense of long scan times associated with multi-dimensional imaging, hindering the adoption of 4D flow MRI into routine clinical imaging. In cardiothoracic applications, the scan times are further increased by the need for respiratory motion compensation, where typically a respiratory navigator follows the movement of the diaphragm, and only accepts data acquired in end-expiration.

In the past decade, compressed sensing (CS), a signal processing technique that efficiently exploits the inherent sparsity of MRI data to recover signals from accelerated measurements, is being used along with various parallel imaging techniques to accelerate 4D flow MRI acquisitions.[18–27] Even though previous studies showed that CS significantly reduced scan times compared to parallel imaging strategies, the clinical translation of this technique was hindered by long offline reconstructions.[18–23,27] Recently, Ma et al demonstrated the feasibility of a CS accelerated 4D flow MRI framework that allowed imaging of the thoracic aorta in under 2 min with inline image reconstruction.[25] While this study evaluated CS-accelerated 4D flow in a pulsatile flow phantom at nine different acceleration factors (R), ranging from R = 5.4 to R = 14.1, the human subject studies were limited to the investigation of one acceleration factor, R = 7.7. Thus, the aim of the current study was to evaluate the performance of the previously developed CS 4D flow MRI framework at three acceleration factors, R = 5.7, 7.7, and 10.2, in a clinical setting. CS 4D flow of the thoracic aorta with these acceleration factors were used to evaluate aortic hemodynamics, including peak velocity (V_{max}), peak flow (Q_{max}), net flow (Q_{net}), and 3D aortic WSS in a prospectively recruited cohort of patients with aortic disease undergoing standard-of-care 4D flow MRI.

2 | METHODS

2.1 | Study cohort

Twenty-five consecutive adult patients with a history of aortic disease (mean age, 58 ± 15 y; range: 21 to 80 y; 19 male/6 female) scheduled for standard-of-care aortic 4D flow MRI

(GRAPPA R = 2) were prospectively recruited between March 2019 and June 2019. Out of the 25 patients, $n = 20$ had aortic root and ascending aortic dilation ($n = 11$ with tricuspid aortic valve [TAV] and $n = 9$ with bicuspid aortic valve [BAV]), $n = 4$ had chronic type-B thoracic aortic dissection and $n = 1$ had mechanical aortic valve replacement with ascending aortic aneurysm repair. The study was approved by the local Institutional Review Board. Written informed consent was obtained from all study participants for the additional research CS 4D flow acquisitions.

2.2 | MRI data acquisition and reconstruction

The 4D flow scans were acquired on a 1.5T MRI system (MAGNETOM Aera; Siemens Healthcare, Erlangen, Germany) following the administration of a gadolinium-based contrast agent (9-28 mL, 0.2 mmol/kg; Gadavist, Bayer Healthcare, Berlin, Germany), received as part of their standard-of-care cardiothoracic MRI. Time between Gd-contrast administration and 4D flow scans varied from 10 to 30 min, depending on the clinical protocol. Standard-of-care 4D flow was acquired with GRAPPA R = 2, while prototype CS accelerated 4D flow scans were acquired at three different acceleration factors, R = 5.7, 7.7, and 10.2. The conventional GRAPPA-accelerated scans were always performed ahead of the CS scans so as to not disrupt the clinical workflow. All four 4D flow scans (one with GRAPPA and three with CS) were acquired with retrospective ECG-triggering during free breathing using navigator-gating and Respiratory Controlled Adaptive k-space Reordering (ReCAR)[28,29] to minimize breathing artifacts. The volumetric coverage, spatiotemporal resolution, and velocity encoding (venc) were matched for all four 4D flow scans. The CS approach in this work used a previously described, Cartesian variable-density phyllotaxis subsampling pattern.[30,31] The CS reconstruction was done by solving the following optimization problem:

$$\{x_t\}_{t=1,\cdots,T} = argmin_{\{x_t\}} \sum_{t=1}^{T} \left(\| A_t x_t - y_t \|_2^2 + \lambda_\sigma \left(\| W_\sigma x_t \|_1 \right) \right) + \lambda_\tau \| W_\tau \{x_1^\intercal, \cdots, x_T^\intercal\} \|_1^T \quad (1)$$

where x_t denotes the frames to be reconstructed all each time points, A_t is the system matrix at each time point, t, and y_t the measured data at each time point. Spatial and temporal L1-regularization was done using Haar wavelet transform where W_σ and W_τ denotes spatial and temporal wavelet transforms and λ_σ and λ_τ the spatial and temporal regularization parameters, respectively.[32] Equation (1) was solved using a FISTA optimization[33] with 30 iterations with $\lambda_\sigma = 0.0015$ and $\lambda_\tau = 5\ \lambda_\sigma$, assuming a maximum image magnitude intensity of 1. To investigate if the number of FISTA iterations used for CS reconstruction was adequate, we performed a sub-analysis on the CS 4D flow MRIs derived from one patient reconstructed at 13 different iterations ranging from 5 to 100. The reconstruction pipeline was integrated into the MRI scanner's data reconstruction workflow. The 4D flow MRI sequence parameters are listed in Table 1.

In addition, the patients also underwent standard-of-care segmented balanced steady-state cine MRI (bSSFP) cine acquisitions at two-chamber, three-chamber, four-chamber, and short-axis orientations. Imaging parameters were as follows: repetition time (TR)/echo time

(TE) = 2.7/1.2 ms; flip angle = 58-70°; voxel size = 2.1 x 2.1 x 8.0 mm^3; slice thickness = 6 mm; bandwidth = 930 Hz/pixel; GRAPPA with R = 2 acceleration. Each myocardial slice was acquired during a breath-hold at end-expiration using retrospective electrocardiograph (ECG)-triggering (with 25 retrospectively constructed cardiac phases).

2.3 | MRI data analysis

4D flow MRI data preprocessing for the conventional and CS 4D flows included inline correction for Maxwell terms[34] and encoding errors due to gradient field distortions.[35] This was followed by offline pre-processing including first-order background phase correction, noise-filtering, and velocity anti-aliasing using in-house software programmed in MATLAB (version R2017b; The MathWorks, Natick, MA, USA).[36–38] A 3D phase-contrast MR angiogram (PC-MRA) was calculated from 4D flow data as previously described.[39] The 3D segmentations of the thoracic aorta were generated to mask the blood flow velocities in the thoracic aorta either manually (Mimics; Materialise, Leuven, Belgium) or automatically using an in-house deep learning-based method.[40] These segmentations were used to create peak-systolic velocity maximum intensity projections (MIPs)[41] to quantify V_{max} in three contiguous regions of interest (ROIs) for each scan: the ascending aorta (AAo), aortic arch (arch), and descending aorta (DAo). For time-resolved flow evaluation and Q_{max} and Q_{net} quantification, three 2D planes were placed orthogonal to the midline at the AAo, arch, and DAo on the segmented volume of the aorta derived from the conventional 4D flow scan (EnSight, version 10.0.3; CEI, Apex, NC, USA). The same planar locations were used for the CS accelerated scans for each patient. Q_{max}, Q_{net}, and flow-waveforms were computed at each of these planes for all 4D flow MRI scans. To account for the slightly different temporal resolutions between the conventional and CS 4D flow MRI, all CS flow data were temporally interpolated using a spline interpolation to the corresponding conventional 4D flow to calculate Q_{max} and Q_{net}. To compare the time-resolved flow across subjects, we temporally interpolated all flow-waveforms to a temporal resolution of 10 ms using a spline interpolation. This interpolated flow-waveforms from each scan at each of the three 2D cross-sectional planes were also averaged over all patients for comparison of flow hemodynamics between the four 4D flow protocols.

The 3D aortic peak WSS was calculated using a previously reported approach[42,43] at six manually defined contiguous ROIs covering the AAo and arch. The WSS measurements were averaged over five cardiac time frames centered at peak-systole to reduce noise, as previously proposed.[43,44] The ROIs were defined by the following landmarks: ROI 1, anterior portion of the region between the sinus of Valsalva and mid-AAo; ROI 2, posterior portion of the region between the sinus of Valsalva and mid-AAo; ROI 3, anterior portion of the region between mid-AAo and the brachiocephalic trunk; ROI 4, posterior portion of the region between mid-AAo and the brachiocephalic trunk; ROI 5, superior portion of the region between the brachiocephalic trunk and left subclavian artery; ROI 6 inferior portion of the region between the brachiocephalic trunk and left subclavian artery. The ratios of the peak WSS at the outer curvature and the inner curvature of the aorta (sum of WSS at ROI1, ROI3, ROI 5 divided by the sum of WSS at ROI2, ROI4, ROI 6) were also calculated to evaluate if the relative changes in regional peak WSS were preserved by the CS 4D flows. The overall 4D flow MRI data analysis workflow is summarized in Figure 1.

To study the effects of acceleration on clinically used cardiac function indicators, as well as, to check for an internal consistency of the 4D flow-derived hemodynamic measurements, we also quantified the stroke volumes (SV) from all 4D flow MRI (total forward flow during cardiac cycle; EnSight) and compared it to the SV derived from the standard bSSFP cine MRI (cvi42; version 5.9, Circle Cardiovascular Imaging, Calgary, Canada).

2.4 | Statistical analysis

For all hemodynamic parameters, a Lilliefors test was used to evaluate normality. The results are expressed as mean ± SD if the parameters were normally distributed and as median (interquartile range) if the parameters had a skewed distribution. A two-tailed paired Student t-test or a Wilcoxon rank-sum test was accordingly applied for comparison of conventional and CS-accelerated scans. Bland-Altman analysis was performed to determine the bias and limits of agreement (bias ± 1.96*SD) between the absolute measurements derived from the four 4D flow scans at different ROIs. To compare the flow-waveforms derived from the different scans, an ANOVA or Freidman test was performed at each time point on the temporally interpolated flow measurements averaged over every subject. For the time-points with significant difference, a paired Student t-test or Wilcoxon rank-sum test was done to identify which CS acceleration factors significantly differed from the conventional GRAPPA-accelerated scan. Bland-Altman analysis and Pearson correlation analysis were performed to compare the SV derived from the 4D flow MRI and the bSSFP cine scans. The statistical significance level was set to $P < .05$.

3 | RESULTS

Out of the 25 patients recruited, 4D flow studies from 21 patients were used for analysis. Scans from three patients had to be excluded due to inaccurate navigator placement and from one patient due to incomplete coverage of the thoracic aortic volume.

3.1 | Effect of number of FISTA iterations

On the sub-analysis on the CS 4D flow MRIs derived from one patient (76-y-old male with aortic root and AAo dilation) reconstructed at 13 different FISTA iterations (range: 5 to 100), we found that all quantified hemodynamic parameters converged around 30 FISTA iterations except for an outlier (Q_{net} at CS, R = 10.2 at the arch showed an increase at 60 iterations and above). Results from this analysis are depicted in Figure 2.

3.2 | Scan times

Average total scan time for the conventional 4D flow MRI was 9:58 ± 2:58 min (4:41 min to 17:3 min), CS 4D flow with R = 5.7 was 3:40 ± 1:19 min (1:25 min to 6:32 min), CS 4D flow with R = 7.7 was 2:50 ± 0:56 min (1:13 min to 4:45 min), and CS 4D flow with R = 10.2 was 2:05 ± 0:42 min (0:54 min to 3:38 min). The average scan times were reduced by 63%, 72%, and 79% for CS 4D flows with R = 5.7, 7.7, and 10.2 respectively ($P < .001$) when compared to the conventional 4D flow.

3.3 | Flow and WSS visualization

Figure 3 depicts an example case, showing the peak-systolic velocity MIPs, 3D WSS vector maps, and 3D streamlines derived from all four 4D flow scans of a 61-y-old patient with aortic root and AAo aneurysm. The velocity distributions of the MIPs and the complex hemodynamic patterns of the 3D streamlines are visually similar between the various scans. Some underestimation of the peak WSS at the AAo by the CS scan (black arrows) can be appreciated in the WSS heat maps.

Visualization of 3D hemodynamics for two patients, one with good agreement and one with poor agreement between the conventional and CS 4D flow (R = 10.2 is shown), is shown in Figure 4. On the left (Figure 4A), analysis from a 76-y-old male with aortic root and AAo dilatation have good agreement overall between CS and conventional GRAPPA data. The velocity magnitude patterns in the MIPs are visually similar and the WSS vectors have similar spatial patterns, although underestimation can be noted in the proximal AAo. Streamline visualization showed similar flow patterns and velocities, although the density of streamlines was reduced with CS data. On the right (Figure 4B), analysis from a 53-y-old male with unoperated chronic type-B aortic dissection had poorer agreement between CS and conventional GRAPPA data. Visible velocity underestimation by the CS 4D flow at the AAo and the true lumen of the DAo can be appreciated in the velocity MIPs, and while 3D aortic WSS vectors showed similar patterns, underestimation can be noted at the AAo and proximal DAo. Blood flow visualization using 3D streamlines showed visibly similar flow patterns, but the velocity magnitudes showed underestimation in the CS data.

3.4 | Flow and WSS quantification

V_{max} was significantly (P = .001 to .039) underestimated at the AAo and arch by all three CS 4D flow protocols when compared to the conventional 4D flow MRI (AAo: underestimation of −5.9 ± 10.3%, −8.2 ± 8.6%, and −7.1 ± 10.0%; arch: −4.5 ± 11.3%, −6.3 ± 14.4%, and −7.3 ± 12.9% by CS, R = 5.7, 7.7, and 10.2, respectively). Bland-Altman analysis for V_{max} (Figure 5A) revealed small negative biases for all three acceleration factors studied (bias of −0.08 m/s, −0.12 m/s, −0.12 m/s for CS, R = 5.7, 7.7, and 10.2, respectively). The SD of the bias remained stable across acceleration factors (0.23 m/s, 0.23 m/s, 0.25 m/s for CS, R = 5.7, 7.7, and 10.2, respectively).

Flow-waveforms averaged over all subjects at the three evaluation planes placed at the AAo, arch, and DAo are shown in Figure 6. The flow-waveforms at each plane showed similar curve shapes, with slight blunting of the curves at every plane by all three CS acquisitions. Statistically significant difference of the time-resolved flow measurements can be appreciated (marked as *) at various time points on the averaged flow-waveforms.

Q_{max} was significantly (P = .001 to .009) underestimated at the arch and DAo by all three CS protocols (arch: underestimation of −6.5 ± 7.2%, −6.9 ± 10.1%, and −7.9 ± 8.1%; DAo: −6.2 ± 7.8%, −8.6 ± 8.1%, and −10.1 ± 9.1%; by CS, R = 5.7, 7.7, and 10.2, respectively). Q_{net} was significantly (P = .006 to .012) underestimated at the arch by all three CS protocols (−7.1 ± 10.5%, −6.8 ± 13.8%, and −5.0 ± 10.7% by CS, R = 5.7, 7.7, and 10.2, respectively) and at the DAo by CS, R = 10.2 (−5.3 ± 11.8%). Evaluation of the Q_{max} and Q_{net} at the AAo

did not reveal any significant underestimation. Bland-Altman analysis for Q_{max} and Q_{net} showed small negative biases for all three acceleration factors (Q_{max}: bias of −12.87 mL/s, −19.44 mL/s, −20.94 mL/s; Q_{net}: bias of −2.52 mL/s, −2.83 mL/s, −3.06 mL/s for CS, R = 5.7, 7.7, and 10.2, respectively) (Figure 5B,C). The SD of the bias for Q_{max} and Q_{net} between the conventional and CS 4D flow MRIs remained consistent across acceleration rates as shown in Figure 5B,C.

In addition, WSS measurements also showed significant (P = .001 to .037) underestimation by the CS 4D flows at all ROIs quantified, with underestimation ranging from −9.0 ± 12.7% to −4.9 ± 10.2% by CS, R = 5.7, −12.3 ± 9.9% to −5.6 ± 10.7% by CS, R = 7.7, and −14.3 ± 12.5% to −8.5 ± 12.6% by CS, R = 10.2. The ratios of the peak WSS were preserved by all three CS acceleration factors, but CS, R = 10.2 showed a trend towards underestimating the WSS at the inner curvature more than the outer curvature of the aorta (outer to inner peak WSS ratios for conventional vs. CS, R = 10.2: 0.94 ± 0.08 vs. 0.98 ± 0.12; P = .057). Bland-Altman analysis showed moderate negative biases for all three acceleration factors (bias of −0.10 Pa, −0.12 Pa, −0.16 Pa for CS, R = 5.7, 7.7, and 10.2, respectively) (Figure 7). The SD of the bias remained relatively stable with CS, R = 10.2 showing higher SD than CS, R = 5.7 and 7.7 (Figure 7).

Table 2 summarizes the regional aortic hemodynamic indices for the different 4D flow techniques.

3.5 | SV quantification

Only 19 out of the 21 subjects included in our analysis underwent bSSFP cardiac cine MRI. The SV derived from 4D flow MRI and bSSFP cine were not significantly different (mean SV from cine: 87.6 ± 21.7 mL/cycle; conventional GRAPPA-accelerated 4D flow: 87.9 ± 23.2 mL/cycle; CS, R = 5.7: 91.3 ± 24.2 mL/cycle; CS, R = 7.7: 89.3 ± 22.9 mL/cycle; CS, R = 10.2: 91.4 ± 20.6 mL/cycle; P = .975). Overall, the measurements from cine and 4D flow MRI showed good agreement (bias: 2.39 mL/cycle; SD of bias: ±8.26 mL/cycle) and correlation (r^2 = .864) (Figure 8).

4 | DISCUSSION

The results from our study demonstrate that: (1) hemodynamic measurements from CS 4D flow MRI with spatial and temporal undersampling at three different acceleration factors studied (R = 5.7, 7.7, and 10.2) plateaus around 30 FISTA iterations; (2) CS 4D flow at all three acceleration factors studied generated data of comparable quality and moderate agreement (mean percent underestimation for regional peak WSS ≤ −9%, −12%, and −14% for R = 5.7, 7.7, and 10.2, respectively) to the conventional GRAPPA-accelerated 4D flow MRI (R = 2); (3) the scan times were significantly reduced by 63%, 72%, and 79% for CS 4D flows with R = 5.7, 7.7, and 10.2, respectively, when compared to the conventional 4D flow MRI with inline image reconstruction at the scanner taking <5 min; (4) the percent underestimation of various hemodynamic parameters increased with increasing acceleration factor, but the changes were relatively lower when compared to the inherent underestimation by CS; (5) among the hemodynamic parameters quantified, Q_{net} was the most stable and WSS was the most sensitive to CS imaging acceleration; (6) clinically utilized cardiac

function indicators like SV could be reliably quantified with all three CS acceleration factors.

The undersampling and reconstruction techniques used in this study were similar to that previously used by Ma et al. The effects of our CS reconstruction techniques, including the number of FISTA iterations, on hemodynamic quantifications were not reported before. Our analysis on one patient dataset reconstructed at a wide range of iterations demonstrates that 30 FISTA iterations resulted in adequate convergence of the data and is suggested for future studies. Effects of other reconstruction parameters like spatial and temporal regularizations were not explored in this study, and further work is required to investigate the effects of spatial and temporal L1-wavelet regularizations.

The underestimation of MRI flow-derived parameters has also been described in previous studies using a CS-based reconstruction approach.[18,20,25,26] Underestimation of hemodynamic measures including V_{max}, Q_{max}, and Q_{net} in our study was also seen in the previous work by Ma et al who used a similar CS 4D flow acquisition framework.[25] The current study further investigated the effects of CS on peak 3D aortic WSS and found increased underestimation compared to the previously studied hemodynamic parameters. This increased underestimation of WSS is likely related to its dependence on spatiotemporal undersampling and regularization.[45–47] The evaluation of the relative changes in regional WSS did not show any significant difference between the conventional and CS 4D flows, except with R = 10.2 CS, which showed a trend toward underestimation of the higher WSS at the inner curvature more than the lower WSS at the outer curvature of the aorta. A detailed comparison of measurements derived from the conventional and CS 4D flow MRIs for each patient are attached as Supporting Information Figure S1, which is available online.

Currently, there are no gold standard diagnostic and prognostic criteria that uses 4D flow-derived hemodynamic parameters in patients with aortic disease. Therefore, it was challenging to understand the clinical significance of hemodynamic underestimation by CS 4D flow when compared to the conventional GRAPPA-accelerated 4D flow. Thus, to evaluate the effects of this underestimation on more clinically relevant cardiac function parameters, we compared the 4D flow-derived SV with bSSFP cine-derived SV (clinical reference standard). We found good correlation and agreement between the two methods for the conventional GRAPPA-accelerated and all three CS 4D flows. This also helped to evaluate the internal consistency of the flow measurements used in the current study.

The scan times for all four 4D flow acquisitions including the conventional 4D flow showed a wide range. This variation in scan times was due in part to dependence on the efficient synchronization of the cardiac and respiratory movements. The heart rates of our cohort ranged from 45 bpm to 97 bpm, and the respiration navigator efficiency ranged from 42% to 98% (mean, 69% ± 16%), resulting in a broad range of recorded scan times. Previous work[29] describing this technique showed a mean navigator efficiency of 63.6% ± 10.5% (range = 47.1-79.6%), which is similar to that of our study. The ReCAR-based navigator gating used in the conventional as well as the CS 4D flow acquisitions has a fixed navigator acceptance window which may have led to this variable navigator efficiencies. Additional methodological development focusing on improving respiratory motion compensation to

have more predictable scan times and increased imaging efficiency would be desirable in clinical workflows.

Recently, Neuhaus et al demonstrated the feasibility of a six- to eight-fold accelerated Cartesian CS aortic 4D flow technique with a scan time of approximately 5 min and an inline reconstruction on the scanner taking around 9 min (Compressed SENSE, Ingenia, Philips Healthcare).[26] A variable-density incoherent undersampling pattern with iterative L1-regularized wavelet-based reconstruction was used along with retrospective ECG triggering and a pencil-beam respiratory navigator. At a CS acceleration factor, R = 8, Neuhaus et al found a statistically significant underestimation of Q_{net} (mean difference of −2.2 ± 7.8 mL/cycle), a trend for underestimation of Q_{max} (mean difference of −4.6 ± 25.2 mL/s), but statistically significant overestimation of V_{max} (mean difference of 7.9 ± 13.0 cm/s) when compared to a conventional SENSE-accelerated 4D flow acquisition. However, temporal correlations were not used in the reconstruction framework of Neuhaus's study, thus not exploiting the full potential of a CS-based reconstruction approach. The differences in the undersampling pattern, regularization, patient populations, and image analysis might have contributed to the lesser significant differences between the conventional and CS approaches in Neuhas's study.

The current study uses both spatial and temporal correlations in a k-t accelerated Cartesian CS 4D flow framework with a variable-density phyllotaxis undersampling and L1-regularized wavelet-based reconstruction. The feasibility of this CS 4D flow framework was demonstrated previously by Ma et al.[25] In patients with aortic disease, Ma et al found that Q_{max} and Q_{net} were underestimated by −6.2 ± 10.4% and −7.1 ± 12.4% at the mid-AAo by this framework at CS, R = 7.7 when compared to GRAPPA, R = 2 aortic 4D flow MRI. The current study found a similar Q_{max} and Q_{net} underestimation of −6.0 ± 9.8% and −3.7 ± 12.0% at CS, R = 7.7. The flow-waveforms averaged for all subjects from the CS 4D flows also showed slight blunting, especially at the peaks in both studies. Ma et al, as well as, the current study found high variability in the degree of underestimation among the patients, seen as high SDs in the results as shown in Table 2 and Figure 5. These high SDs remained stable with increasing CS acceleration. This may be due to the heterogeneous aortic hemodynamics in the small patient cohorts studied, variability in imaging parameters (venc-dependent phase noise etc.), and variability in the uncontrolled effects during the scan (e.g. movement, heart-rate/respiratory variability). Future studies on larger cohorts are warranted to assess the effects of different venc and find other factors influencing this variability in underestimation.

Our study has several limitations. First, the study was conducted on a small and heterogeneous patient population studied at a single center. While the majority of the patients had thoracic aortic aneurysms with TAV or BAV, 20% of our patients had chronic aortic dissections and resulting complex blood flow hemodynamics, which would have influenced our results. Second, the three CS 4D flow scans were added on to the standard-of-care CMR and was always acquired at the end of the session, immediately after the conventional GRAPPA-accelerated 4D flow acquisition. There is a possibility that this would have led to improved SNRs in the conventional GRAPPA scans influencing our

results. But we expect this to have lesser impact considering that all four scans were performed approximately 10–30 min following contrast administration.

Third, the temporal resolutions slightly varied between the GRAPPA and the CS 4D flow scans. This was due to variations in the number of reconstructed cardiac time frames. The k-space data from the conventional GRAPPA-accelerated 4D flow MRI were always retrospectively reconstructed to yield 30 cardiac time frames as per our standard-of-care protocol (ie, the acquired temporal resolution was different from reconstructed temporal resolution). In contrast, the number of cardiac time frames for the CS accelerated 4D flow MRI scans had to be adapted to the subject's heart rate to account for pseudo random sampling, which did not allow for retrospective interpolation to 30 time frames. If the reconstructed cardiac time frames were not changed based on the subject's heart rate, the actual acceleration factor would not match the acceleration factor reported on the user interface. To account for this, we had to temporally interpolate (spline interpolation) the flow data from all CS accelerated 4D flow scans to the corresponding conventional GRAPPA-accelerated 4D flow MRI. This might have introduced errors in results.

Fourth, the analysis approach for V_{max}, flow, and WSS differed based on previously validated techniques.[43,44,48,49] This was mostly because without the corrections used in these techniques the calculations, especially peak measurements, would be impacted heavily by noise. Fifth, the current study did not do a systematic analysis of the effects of different spatial and temporal resolutions in the CS 4D flow image quality or hemodynamics. Since spatiotemporal resolutions are known to impact the assessment of parameters like WSS, [45–47,50] future studies should be conducted to investigate their effects on CS 4D flow derived hemodynamics. Sixth, the effects of various regularization strategies were not explored in this study. The results from our study indicate that the effects of acceleration on hemodynamic quantification might be less pronounced when compared to that inherently induced by CS. An in-depth analysis into the effects of regularization strategies has to be evaluated in future studies.

5 | CONCLUSIONS

In conclusion, this study demonstrates that highly accelerated CS 4D flow MRI of the thoracic aorta at acceleration factors, R = 5.7, 7.7, and 10.2 generated data of moderate agreement to the conventional GRAPPA, R = 2 accelerated 4D flow MRI. The choice of CS acceleration factor to use depends on the clinical question at hand, striking a balance between shorter scan times and the need for accurate hemodynamic quantification. In either case, CS 4D flow can be used as a high-throughput method to evaluate aortic hemodynamics in routine clinical practice. Further investigations should be carried out in a larger multi-centric patient population to establish reference normal ranges for aortic hemodynamic parameters using CS 4D flow.

Supplementary Material

Refer to Web version on PubMed Central for supplementary material.

Acknowledgments

Funding information Grant support by NIH F30 HL137279, NIH F30 HL145995, R01HL115828.

CONFLICT OF INTEREST

The Department of Radiology has research agreements with Siemens Medical Solutions USA, Inc. The following authors are employees: KC (Siemens Medical Solutions USA, Inc.); CF (Siemens Healthcare); NJ (Siemens Medical Solutions USA, Inc.). JC receives institutional research grants from Siemens, Bayer, and Guerbet, speaker honoraria from Bayer and is on the advisory boards of Siemens, Bayer, and Bracco. MM receives research support from Siemens, research grants from Circle Cardiovascular Imaging and Cryolife Inc., and is a consultant for Circle Cardiovascular Imaging. The other authors have no conflict of interest to disclose. The authors declare that the research was conducted in the absence of any commercial or financial relationships that could be construed as a potential conflict of interest.

REFERENCES

1. Vasanawala SS, Hanneman K, Alley MT, Hsiao A. Congenital heart disease assessment with 4D flow MRI. J Magn Reson Imaging. 2015;42:870–886. [PubMed: 25708923]
2. Lawley CM, Broadhouse KM, Callaghan FM, Winlaw DS, Figtree GA, Grieve SM. 4D flow magnetic resonance imaging: Role in pediatric congenital heart disease. Asian Cardiovasc Thorac Ann. 2018;26:28–37. [PubMed: 28185475]
3. Markl M, Geiger J, Kilner PJ, et al. Time-resolved three-dimensional magnetic resonance velocity mapping of cardiovascular flow paths in volunteers and patients with Fontan circulation. Eur J Cardiothorac Surg. 2011;39:206–212. [PubMed: 20598560]
4. Valverde I, Nordmeyer S, Uribe S, et al. Systemic-to-pulmonary collateral flow in patients with palliated univentricular heart physiology: Measurement using cardiovascular magnetic resonance 4D velocity acquisition. J Cardiovasc Magn Reson. 2012;14:25. [PubMed: 22541134]
5. Binter C, Gotschy A, Sundermann SH, et al. Turbulent kinetic energy assessed by multipoint 4-dimensional flow magnetic resonance imaging provides additional information relative to echocardiography for the determination of aortic stenosis severity. Circ Cardiovasc Imaging. 2017;10:e005486. [PubMed: 28611119]
6. Driessen MMP, Schings MA, Sieswerda GT, et al. Tricuspid flow and regurgitation in congenital heart disease and pulmonary hypertension: Comparison of 4D flow cardiovascular magnetic resonance and echocardiography. J Cardiovasc Magn Reson. 2018;20:5. [PubMed: 29332606]
7. Roes SD, Hammer S, van der Geest RJ, et al. Flow assessment through four heart valves simultaneously using 3-dimensional 3-directional velocity-encoded magnetic resonance imaging with retrospective valve tracking in healthy volunteers and patients with valvular regurgitation. Invest Radiol. 2009;44:669–675. [PubMed: 19724233]
8. Eriksson J, Bolger AF, Ebbers T, Carlhall CJ. Four-dimensional blood flow-specific markers of LV dysfunction in dilated cardiomyopathy. Eur Heart J Cardiovasc Imaging. 2013;14:417–424. [PubMed: 22879457]
9. Burris NS, Hope MD. 4D flow MRI applications for aortic disease. Magn Reson Imaging Clin. 2015;23:15–23.
10. Bissell MM, Loudon M, Hess AT, et al. Differential flow improvements after valve replacements in bicuspid aortic valve disease: A cardiovascular magnetic resonance assessment. J Cardiovasc Magn Reson. 2018;20:10. [PubMed: 29422054]
11. Garcia J, Barker AJ, Markl M. The role of imaging of flow patterns by 4D flow MRI in aortic stenosis. JACC Cardiovasc Imaging. 2019;12:252–266. [PubMed: 30732721]
12. Hope MD, Meadows AK, Hope TA, et al. Clinical evaluation of aortic coarctation with 4D flow MR imaging. J Magn Reson Imaging. 2010;31:711–718. [PubMed: 20187217]
13. Rahman O, Markl M, Balte P, et al. Reproducibility and changes in vena caval blood flow by using 4D flow MRI in pulmonary emphysema and chronic obstructive pulmonary disease (COPD): The multi-ethnic study of atherosclerosis (MESA) copd substudy. Radiology. 2019;292:585–594. [PubMed: 31335282]

14. Fatehi Hassanabad A, Burns F, Bristow MS, et al. Pressure drop mapping using 4D flow MRI in patients with bicuspid aortic valve disease: A novel marker of valvular obstruction. Magn Reson Imaging. 2020;65:175–182. [PubMed: 31726212]
15. Jarvis K, Pruijssen JT, Son AY, et al. Parametric hemodynamic 4D flow MRI maps for the characterization of chronic thoracic descending aortic dissection. J Magn Reson Imaging. 2020;51:1357–1368. [PubMed: 31714648]
16. van Amerom JFP, Lloyd DFA, Deprez M, et al. Fetal whole-heart 4D imaging using motion-corrected multi-planar real-time MRI. Magn Reson Med. 2019;82:1055–1072. [PubMed: 31081250]
17. Harloff A, Hagenlocher P, Lodemann T, et al. Retrograde aortic blood flow as a mechanism of stroke: MR evaluation of the prevalence in a population-based study. Eur Radiol. 2019;29:5172–5179. [PubMed: 30877458]
18. Hsiao A, Lustig M, Alley MT, Murphy MJ, Vasanawala SS. Evaluation of valvular insufficiency and shunts with parallel-imaging compressed-sensing 4D phase-contrast MR imaging with stereoscopic 3D velocity-fusion volume-rendered visualization. Radiology. 2012;265:87–95. [PubMed: 22923717]
19. Basha TA, Akçkaya M, Goddu B, Berg S, Nezafat R. Accelerated three-dimensional cine phase contrast imaging using randomly undersampled echo planar imaging with compressed sensing reconstruction. NMR Biomed. 2015;28:30–39. [PubMed: 25323208]
20. Dyvorne H, Knight-Greenfield A, Jajamovich G, et al. Abdominal 4D flow MR imaging in a breath hold: Combination of spiral sampling and dynamic compressed sensing for highly accelerated acquisition. Radiology. 2015;275:245–254. [PubMed: 25325326]
21. Cheng JY, Hanneman K, Zhang T, et al. Comprehensive motion-compensated highly accelerated 4D flow MRI with ferumoxytol enhancement for pediatric congenital heart disease. J Magn Reson Imaging. 2016;43:1355–1368. [PubMed: 26646061]
22. Rich A, Potter LC, Jin N, Liu Y, Simonetti OP, Ahmad R. A Bayesian approach for 4D flow imaging of aortic valve in a single breath-hold. Magn Reson Med. 2019;81:811–824. [PubMed: 30265770]
23. Valvano G, Martini N, Huber A, et al. Accelerating 4D flow MRI by exploiting low-rank matrix structure and hadamard sparsity. Magn Reson Med. 2017;78:1330–1341. [PubMed: 27787911]
24. Jin N, Ma L, Chow K, et al. Highly-Accelerated 4D flow in the aorta with compressed sensing, respiratory controlled adaptive k-Space reordering and inline reconstruction. In: Proceedings of the 26th Annual Meeting of the ISMRM, Paris, France 2018 Abstract 0687.
25. Ma LE, Markl M, Chow K, et al. Aortic 4D flow MRI in 2 minutes using compressed sensing, respiratory controlled adaptive k-space reordering, and inline reconstruction. Magn Reson Med. 2019;81:3675–3690. [PubMed: 30803006]
26. Neuhaus E, Weiss K, Bastkowski R, Koopmann J, Maintz D, Giese D. Accelerated aortic 4D flow cardiovascular magnetic resonance using compressed sensing: applicability, validation and clinical integration. J Cardiovasc Magn Reson. 2019;21:65. [PubMed: 31638997]
27. Gottwald LM, Peper ES, Zhang Q, et al. Pseudo-spiral sampling and compressed sensing reconstruction provides flexibility of temporal resolution in accelerated aortic 4D flow MRI: A comparison with k-t principal component analysis. NMR Biomed. 2020;33:e4255. [PubMed: 31957927]
28. Bailes DR, Gilderdale DJ, Bydder GM, Collins AG, Firmin DN. Respiratory ordered phase encoding (ROPE): A method for reducing respiratory motion artefacts in MR imaging. J Comput Assist Tomogr. 1985;9:835–838. [PubMed: 4019854]
29. Markl M, Harloff A, Bley TA, et al. Time-resolved 3D MR velocity mapping at 3T: Improved navigator-gated assessment of vascular anatomy and blood flow. J Magn Reson Imaging. 2007;25:824–831. [PubMed: 17345635]
30. Uecker M, Lai P, Murphy MJ, et al. ESPIRiT–an eigenvalue approach to autocalibrating parallel MRI: Where SENSE meets GRAPPA. Magn Reson Med. 2014;71:990–1001. [PubMed: 23649942]

31. Forman C, Piccini D, Grimm R, Hutter J, Hornegger J, Zenge MO. High-resolution 3D whole-heart coronary MRA: A study on the combination of data acquisition in multiple breath-holds and ID residual respiratory motion compensation. Magma. 2014;27:435–443. [PubMed: 24402560]
32. Wetzl J, Forman C, Wintersperger BJ, et al. High-resolution dynamic CE-MRA of the thorax enabled by iterative TWIST reconstruction. Magn Reson Med. 2017;77:833–840. [PubMed: 26888549]
33. Beck A, Teboulle M. A fast iterative shrinkage-thresholding algorithm for linear inverse problems. SIAM Journal on Imaging Sciences. 2009;2:183–202.
34. Bernstein MA, Zhou XJ, Polzin JA, et al. Concomitant gradient terms in phase contrast MR: Analysis and correction. Magn Reson Med. 1998;39:300–308. [PubMed: 9469714]
35. Markl M, Bammer R, Alley MT, et al. Generalized reconstruction of phase contrast MRI: Analysis and correction of the effect of gradient field distortions. Magn Reson Med. 2003;50:791–801. [PubMed: 14523966]
36. Bock J, Kreher BW, Hennig J, Markl M. Optimized pre-processing of time-resolved 2D and 3D phase contrast MRI data. In: Proceedings of the 15th Annual Meeting of ISMRM 2007 Abstract 3138.
37. Busch J, Giese D, Kozerke S. Image-based background phase error correction in 4D flow MRI revisited. J Magn Reson Imaging. 2017;46:1516–1525. [PubMed: 28225577]
38. Walker PG, Cranney GB, Scheidegger MB, Waseleski G, Pohost GM, Yoganathan AP. Semiautomated method for noise reduction and background phase error correction in MR phase velocity data. J Magn Reson Imaging. 1993;3:521–530. [PubMed: 8324312]
39. Schnell S, Entezari P, Mahadewia RJ, et al. Improved semiautomated 4D flow MRI analysis in the aorta in patients with congenital aortic valve anomalies versus tricuspid aortic valves. J Comput Assist Tomogr. 2016;40:102–108. [PubMed: 26466113]
40. Berhane H, Scott M, Elbaz M, et al. Fully automated 3D aortic segmentation of 4D flow MRI for hemodynamic analysis using deep learning. Magn Reson Med. 2020;84:2204–2218. [PubMed: 32167203]
41. Rose MJ, Jarvis K, Chowdhary V, et al. Efficient method for volumetric assessment of peak blood flow velocity using 4D flow MRI. J Magn Reson Imaging. 2016;44:1673–1682. [PubMed: 27192153]
42. Potters WV, van Ooij P, Marquering H, vanBavel E, Nederveen AJ. Volumetric arterial wall shear stress calculation based on cine phase contrast MRI. J Magn Reson Imaging. 2015;41:505–516. [PubMed: 24436246]
43. van Ooij P, Potters WV, Nederveen AJ, et al. A methodology to detect abnormal relative wall shear stress on the full surface of the thoracic aorta using four-dimensional flow MRI. Magn Reson Med. 2015;73:1216–1227. [PubMed: 24753241]
44. Bollache E, Fedak PWM, van Ooij P, et al. Perioperative evaluation of regional aortic wall shear stress patterns in patients undergoing aortic valve and/or proximal thoracic aortic replacement. J Thorac Cardiovasc Surg. 2018;155:2277–2286.e2272. [PubMed: 29248286]
45. Cibis M, Potters WV, Gijsen FJH, et al. Wall shear stress calculations based on 3D cine phase contrast MRI and computational fluid dynamics: A comparison study in healthy carotid arteries. NMR Biomed. 2014;27:826–834. [PubMed: 24817676]
46. Potters WV, van Ooij P, Marquering H, vanBavel E, Nederveen AJ. Volumetric arterial wall shear stress calculation based on cine phase contrast MRI. J Magn Reson Imaging. 2015;41:505–516. [PubMed: 24436246]
47. Zimmermann J, Demedts D, Mirzaee H, et al. Wall shear stress estimation in the aorta: Impact of wall motion, spatiotemporal resolution, and phase noise. J Magn Reson Imaging. 2018;48:718–728.
48. Rose MJ, Jarvis K, Chowdhary V, et al. Efficient method for volumetric assessment of peak blood flow velocity using 4D flow MRI. J Magn Reson Imaging. 2016;44:1673–1682. [PubMed: 27192153]
49. Bollache E, Knott KD, Jarvis K, et al. Two-minute k-space and time-accelerated aortic four-dimensional flow MRI: Dual-center study of feasibility and impact on velocity and wall shear stress quantification. Radiology Cardiothoracic Imaging. 2019;1:e180008. [PubMed: 32076666]

50. Jaspan ON, Fleysher R, Lipton ML. Compressed sensing MRI: a review of the clinical literature. Br J Radiol. 2015;88:20150487. [PubMed: 26402216]

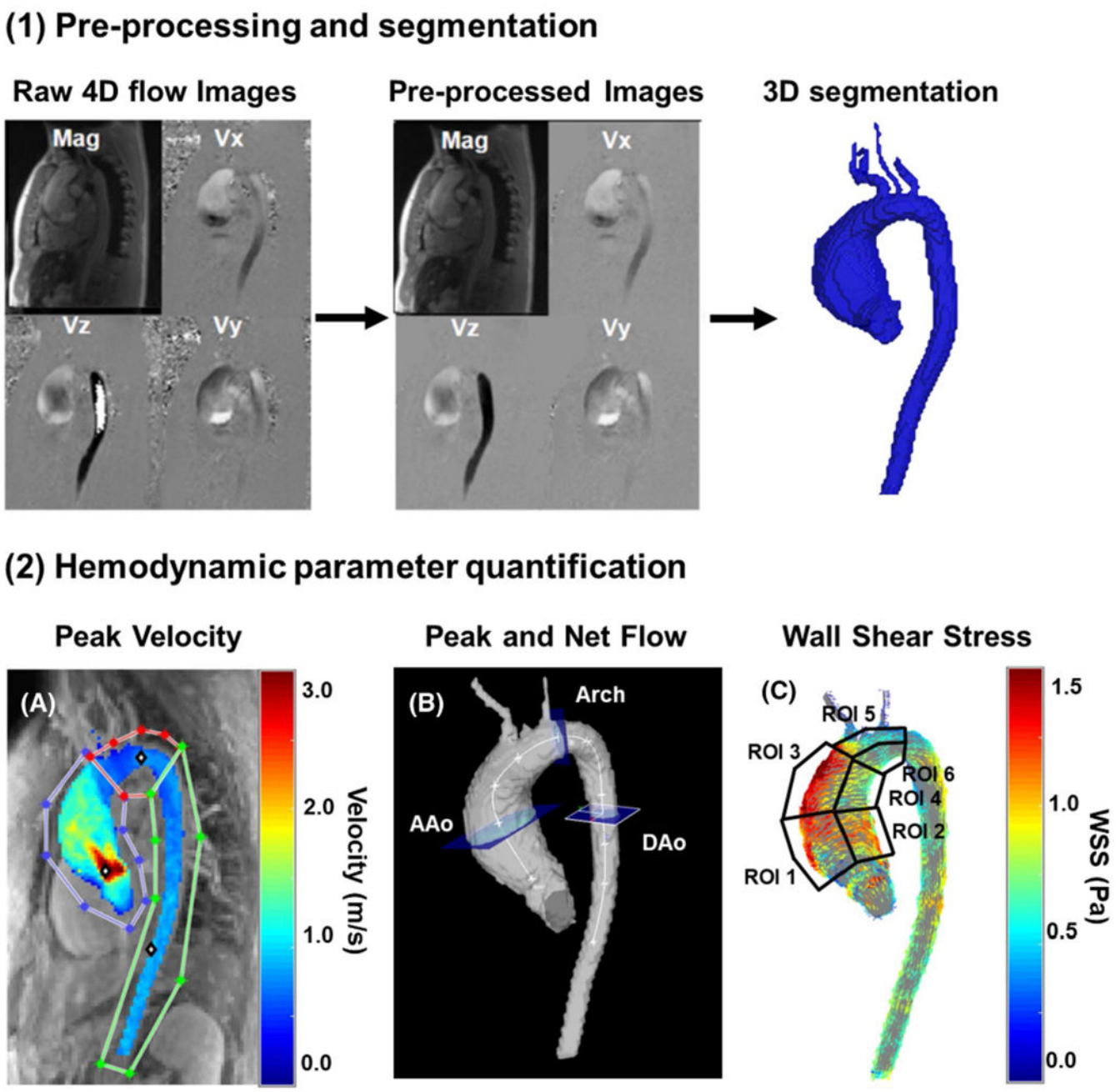

FIGURE 1.

The 4D flow MRI analysis workflow. (1) Raw 4D flow MRI images were pre-processed by noise filtering, eddy-current corrections, and anti-aliasing, followed by 3D aortic segmentation either manually or using an in-house auto-segmentation tool. (2) A, V_{max} was measured by manually defining ROIs at the AAo, arch, and DAo on the peak-systolic velocity Maximum Intensity Projections (MIPs). The MIPs were eroded by one pixel to suppress border noise. B, Q_{max} and Q_{net} were measured by placing three matching analysis planes (AAo, arch, and DAo) for the four 4D flow scans from each patient. C, Peak-systolic 3D aortic WSS was measured at 6 ROIs as shown

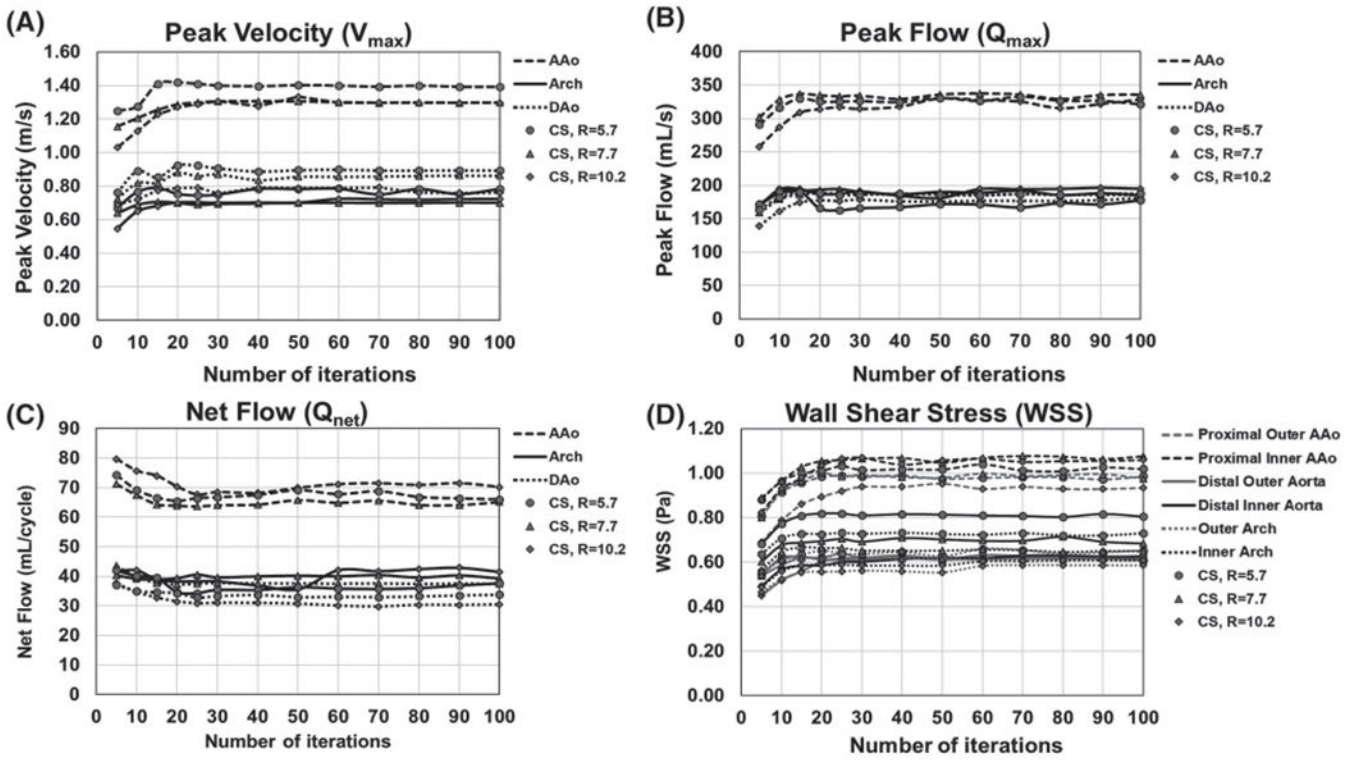

FIGURE 2.

Hemodynamic quantification results from CS 4D flow MRI (R = 5.7, R = 7.7, and R = 10.2) reconstructed at 13 different FISTA iterations. A, Peak velocities (V_{max}). B, Peak flow (Q_{max}). C, Net flow (Q_{net}). and D, WSS results are shown. Except for an outlier dataset (Q_{net} at CS, R = 10.2 at the arch) that showed an increase in measurements at 60 iterations and above, we found that all other quantifications converged around 30 FISTA iterations

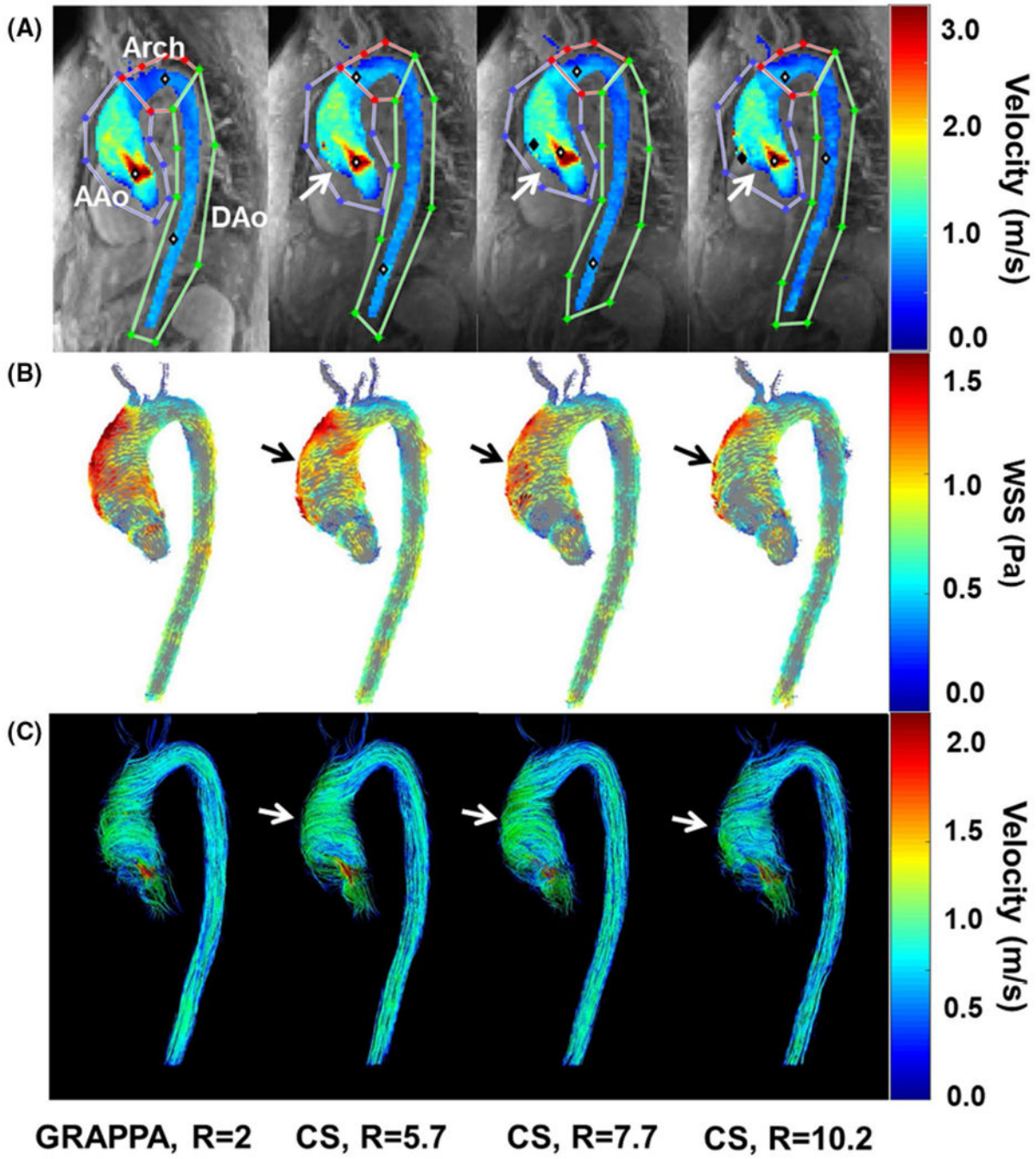

FIGURE 3.

Examples comparing conventional and CS 4D flow scans. A, Systolic velocity maximum Intensity projections (MIPs) derived from the conventional and CS 4D flow MRIs of a representative patient showing similar velocity patterns of the systolic jet (arrows). (◊) represent points of peak velocity at each ROI and (♦) represent noised pixels that were excluded. B, Posterior-right view of the aortic WSS vector maps from the same patient showing similar patterns, but underestimation marked by arrows. C, Peak-systolic 3D streamlines derived from the conventional and CS 4D flows for the same patient. The

complex flow patterns in the AAo is very well captured by the CS 4D flow scans, without any visually apparent underestimation in streamline velocities (arrows)

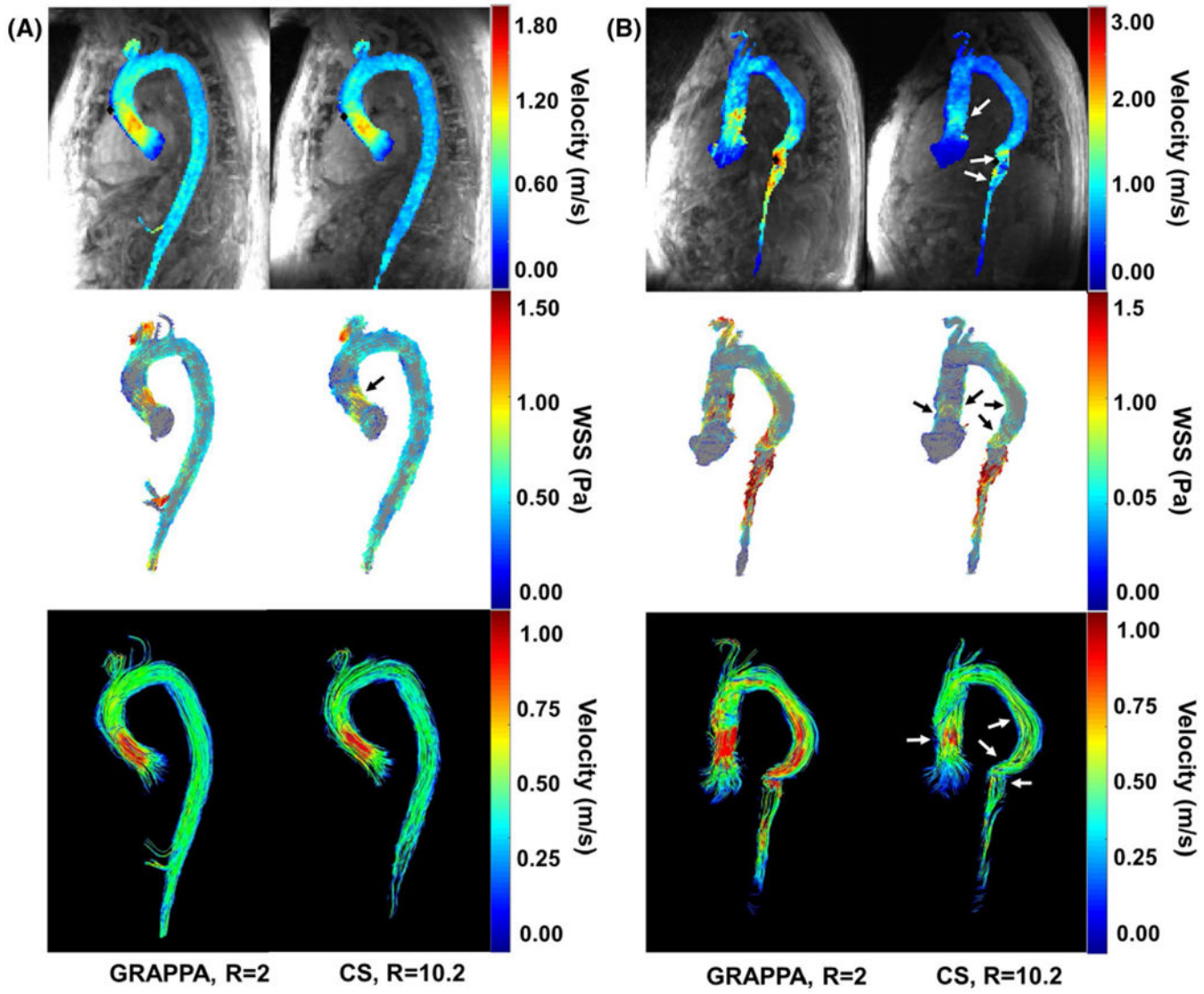

FIGURE 4.

Representative aortic hemodynamics of two patients, one with good agreement and one with poor agreement between the CS and conventional 4D flow. Panel A shows systolic velocity MIPs, WSS vector maps, and 3D streamlines from the GRAPPA, R = 2, and CS, R = 10.2 4D flow scans from a 76-y-old male with aortic root and AAo dilation. There is good similarity between the velocity magnitude distribution on the MIPs and the 3D streamlines patterns, with some underestimation of WSS at the AAo. Panel B shows the results from a 53-y-old male with unoperated chronic type-B thoracic aortic dissection. The differences in the systolic velocity MIPs can be well appreciated at the proximal AAo and the true lumen. WSS vector maps also show decreased measures at the proximal AAo in the CS 4D flow when compared to the GRAPPA 4D flow. The flow visualization using 3D streamlines also shows underestimation by the CS 4D flow

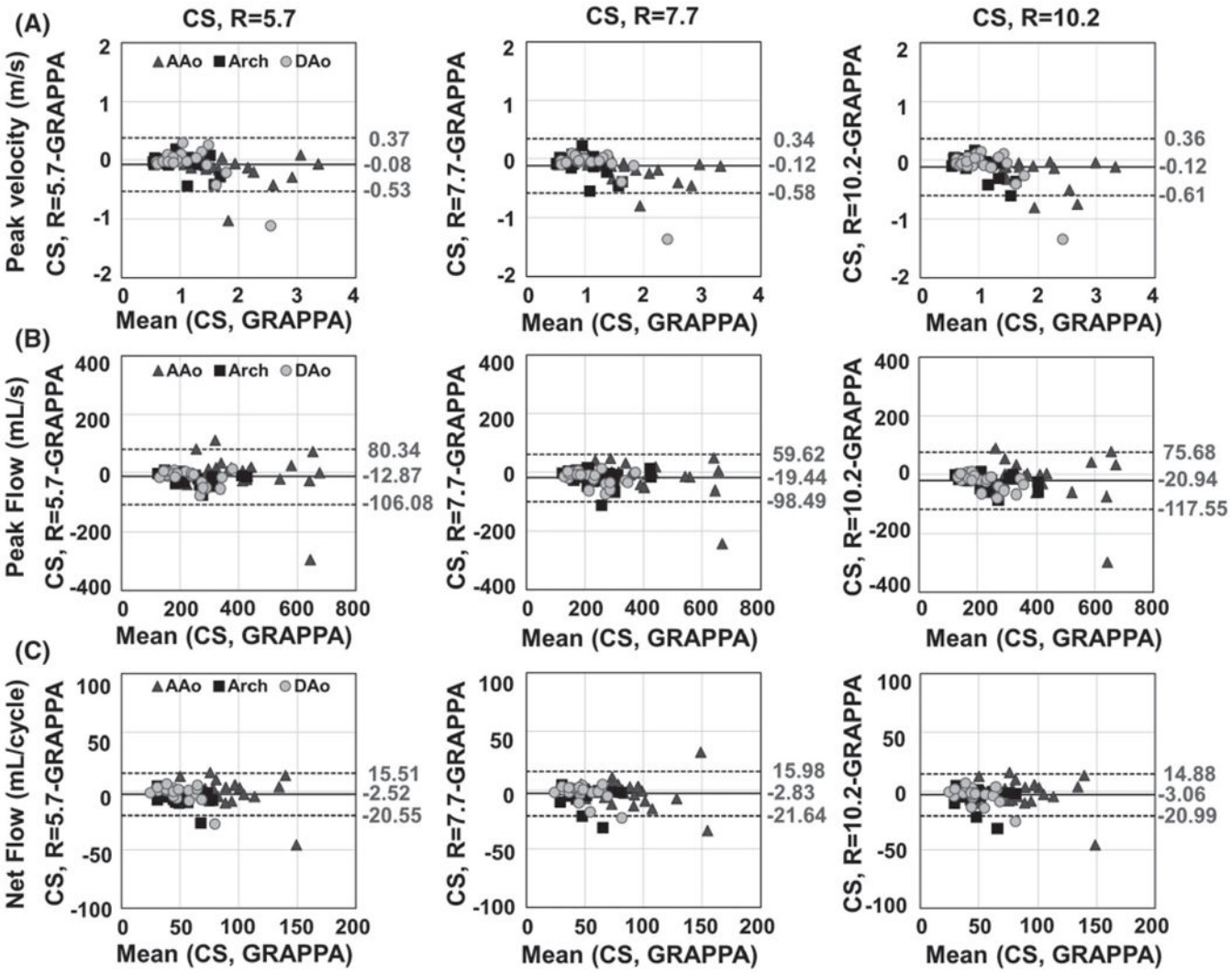

FIGURE 5.

Bland-Altman plots comparing the measurements from the conventional and CS 4D flow scans for the V_{max} (A), Q_{max} (B), and Q_{net} (C). Data from the AAo, arch, and DAo are marked by different markers. The mean differences and 95% confidence intervals were calculated from the measurements from all ROIs. We can see that the small negative bias for V_{max}, Q_{max}, and Q_{net} increase with increasing CS acceleration factor, while the SDs remain relatively stable

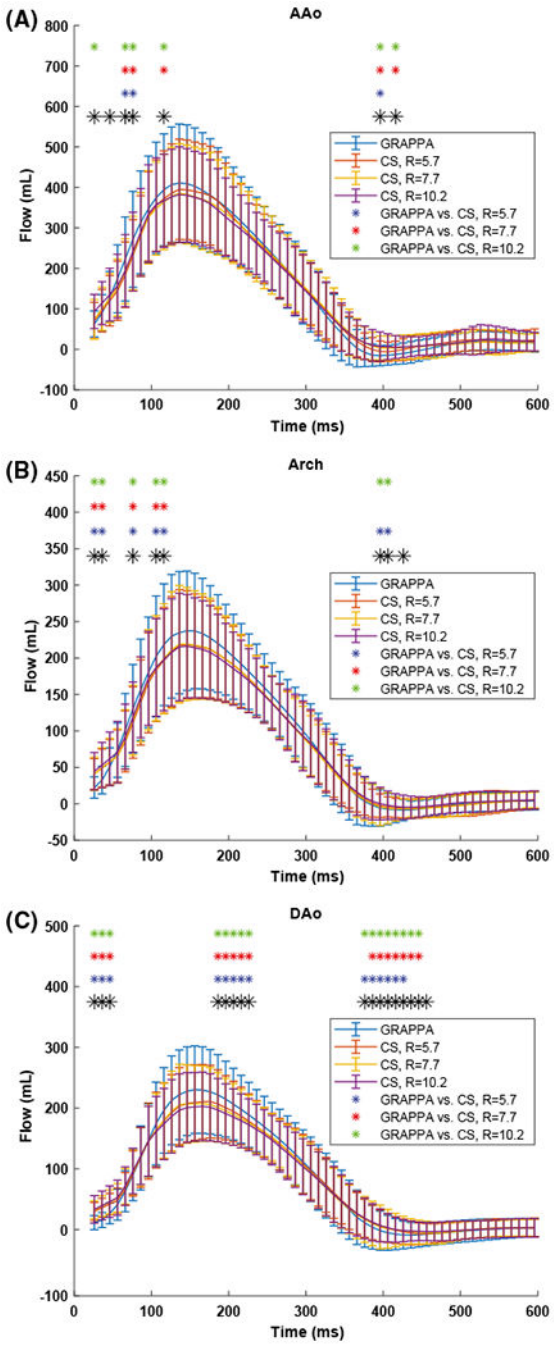

FIGURE 6.

Flow-waveforms from the conventional and CS 4D flow scans averaged over all subjects at matched planes placed at the AAo, arch, and DAo. Each curve shows the time-resolved flow measurements averaged over all subjects and their standard error of the mean as error bars. Black (*) indicates time-points with significant differences ($P < .05$; ANOVA or Freidman test) between the measurements obtained from the four 4D flow techniques. Colored (*) indicates time-points with significant differences ($P < .05$; paired Student t-tests/Wilcoxon rank-sum tests) between GRAPPA and different CS 4D flows (blue: CS, R = 5.7; red: CS, R

= 7.7; green: CS, R = 10.2). Similar flow patterns with mild underestimation of the Q_{max} seen as blunting of the peaks by all three CS acceleration factors can be seen

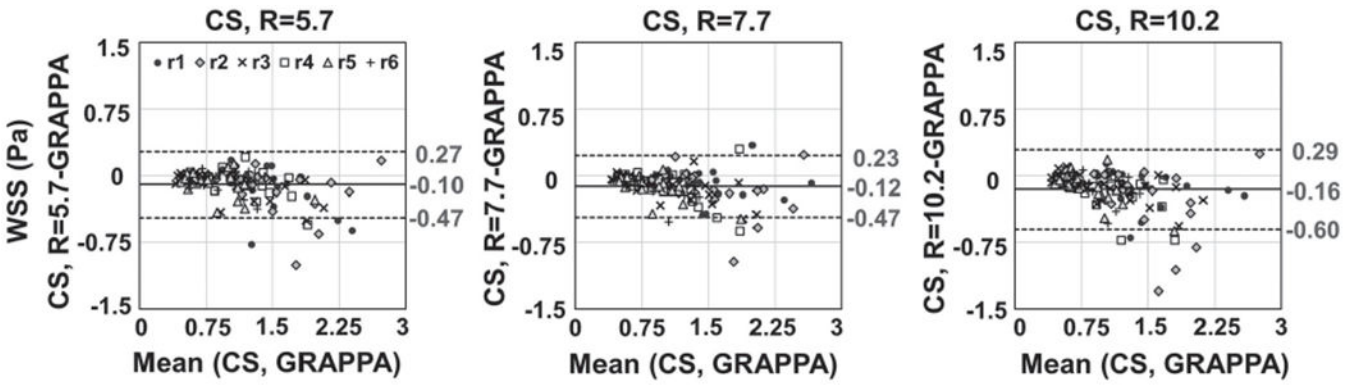

FIGURE 7.

Bland-Altman plots comparing the measurements from the conventional and CS 4D flow scans for the WSS quantifications. The small-to-moderate negative bias increases with increasing acceleration. Data from the six different ROIs are marked by different markers. r1, proximal outer AAo; r2, proximal inner AAo; r3, distal outer AAo; r4, distal inner AAo; r5, outer arch; r6, inner arch

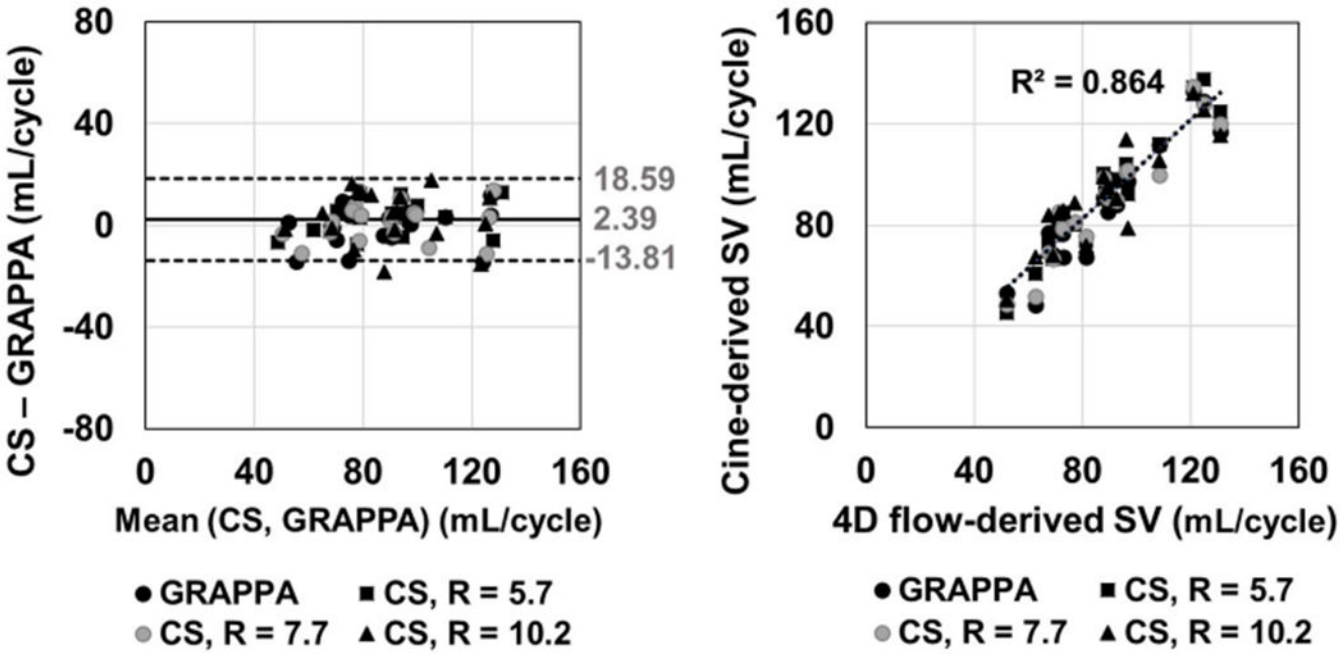

FIGURE 8.

Bland-Altman and Pearsons correlation plots comparing the stroke volumes derived from all four 4D flow MRI with that derived from bSSFP cine MRI. There was good agreement and correlation between the measurements derived from both techniques

TABLE 1

Imaging parameters for conventional and CS accelerated 4D flow MRI

Imaging acceleration technique	**Parallel imaging (GRAPPA)**	**CS**		
Acceleration rate, R	2	5.7	7.7	10.2
Scan time (min)	9:58 ± 2:58	3:40 ± 1:19	2:50 ± 0:56	2:05 ± 0:42
Repetition time (ms)	5.0 (4.8-5.1)	5.0 (4.8-5.1)		
Echo time (ms)	2.3 (2.1-2.3)	2.2 (2.1-2.3)		
Field of view (mm^3)	380-450 × 285-374 × 72-140	380-450 × 285-374 × 72-140		
Spatial resolution (mm^3)	3.6-4.2 × 2.4-2.8 × 2.4-3.5	3.6-4.3 × 2.4-2.8 × 2.4-3.5		
Temporal resolution (ms)	38.6-40.6	38.5-40.5		
Receiver bandwidth (Hz/pixel)	455	455		
Flip angle (°)	15	15		
Velocity encoding (cm/s)	150-350	150-350		
Navigator window (mm)	±8	±8		
Reconstructed cardiac phases	20-30	15-33		

TABLE 2

Comparison between the V_{max}, Q_{max}, Q_{net}, and 3D aortic WSS derived from conventional 4D flow and CS accelerated 4D flows at different acceleration factors.

		GRAPPA, R = 2	CS, R = 5.7	*P*-value	CS, R = 7.7	*P*-value	CS, R = 10.2	*P*-value
V_{max} (m/s)	AAo	1.9 ± 0.7	1.7 ± 0.7	<0.01	1.7 ± 0.6	<0.01	1.7 ± 0.6	<.01
	Arch	1.0 ± 0.4	0.9 ± 0.3	0.04	0.9 ± 0.3	0.03	0.9 ± 0.3	.01
	DAo	1.1 ± 0.6	1.1 ± 0.4	0.85	1.0 ± 0.4	0.05	1.0 ± 0.4	.12
Q_{max} (mL/s)	AAo	427 ± 159	423 ± 134	0.88	409 ± 137	0.17	413 ± 136	.79
	Arch	246 ± 86	228 ± 80	<0.01	228 ± 83	0.01	224 ± 77	<.01
	DAo	239 ± 77	222 ± 68	<0.01	217 ± 68	<0.01	211 ± 61	<.01
Q_{net} (mL/cycle)	AAo	92 ± 29	91 ± 25	0.64	90 ± 27	0.48	89 ± 23	.37
	Arch	52 ± 15	47 ± 13	0.01	48 ± 14	0.03	49 ± 14	.01
	DAo	50 ± 16	48 ± 12	0.22	47 ± 13	0.15	46 ± 13	.04
WSS (Pa)	ROI 1	1.5 ± 0.5	1.3 ± 0.4	0.03	1.4 ± 0.5	0.03	1.3 ± 0.5	<.01
	ROI 2	1.6 ± 0.5	1.4 ± 0.5	0.02	1.4 ± 0.5	0.01	1.3 ± 0.5	.01
	ROI 3	1.1 ± 0.6	1.0 ± 0.5	0.01	1.0 ± 0.5	<0.01	1.0 ± 0.5	<.01
	ROI 4	1.1 ± 0.5	1.0 ± 0.4	0.04	1.0 ± 0.4	0.01	0.9 ± 0.4	<.01
	ROI 5	0.9 ± 0.4	0.8 ± 0.3	0.01	0.8 ± 0.3	<0.01	0.8 ± 0.3	<.01
	ROI 6	0.9 ± 0.3	0.9 ± 0.3	0.02	0.8 ± 0.3	<0.01	0.8 ± 0.2	<.01

% change indicates the % difference relative to the conventional, GRAPPA R = 2 4D flow.